JOURNAL OF CHEMICAL & ENGINEERING DATA

ARTICLE

pubs.acs.org/jced

Evaluation of Polymers as Direct Thickeners for CO_2 Enhanced Oil Recovery

Shiyang Zhang,[†] Yuehui She,[‡] and Yongan Gu*[,†]

[†]Petroleum Technology Research Centre (PTRC), Petroleum Systems Engineering, Faculty of Engineering and Applied Science, University of Regina, Regina, Saskatchewan S4S 0A2, Canada

[‡]College of Chemical and Environmental Engineering, Yangtze University, Jingzhou, Hubei 434023, P. R. China

ABSTRACT: In this paper, two commercial polymers, poly(vinyl ethyl ether) (PVEE) and poly(1-decene) (P-1-D), are tested to thicken CO_2 for CO_2 enhanced oil recovery (EOR). First, a series of laboratory tests are conducted to measure the cloud-point pressures of either polymer at different polymer solubilities in supercritical CO_2 and the equilibrium interfacial tensions (IFTs) of a light crude oil-pure or polymer-thickened CO_2 system under different reservoir conditions. Second, a capillary viscometer is used to measure the viscosities of polymer-thickened CO_2 at different test pressures. Third, a total of six high-pressure CO_2 coreflood tests are performed to examine the effects of polymer-thickened CO_2 on the total CO_2 EOR. It is found that at the same and low polymer solubility in pure CO_2, the measured cloud-point pressure of PVEE is much lower than that of P-1-D. The measured equilibrium IFT for polymer-thickened CO_2 at a high pressure is much lower than that for pure CO_2. The PVEE- or P-1-D-thickened CO_2 viscosity is approximately (13 to 14) times higher than the pure CO_2 viscosity. The CO_2 coreflood test results show that PVEE- or P-1-D-thickened CO_2 flooding can further enhance oil recovery after a pure CO_2 breakthrough. The CO_2 breakthrough can be significantly delayed if polymer-thickened CO_2 is injected directly.

INTRODUCTION

Enhanced oil recovery (EOR) processes have become increasingly important to the petroleum industry. After the primary and secondary oil recovery, a typical residual oil saturation in a light or medium oil reservoir is still in the range of (50 to 60) % of the original-oil-in-place (OOIP).[1] Thus the subsequent EOR processes contribute significantly to the overall oil production. Among all of the EOR methods developed for the light and/or medium oil reservoirs, carbon dioxide (CO_2) flooding has been successful to a large extent under some favorable reservoir conditions.[2] It is worthwhile to emphasize that CO_2 flooding not only effectively enhances oil recovery[3] but also considerably reduces greenhouse gas emissions.[4]

It is well-known that one of the major technical challenges related to CO_2 flooding is its mobility control. The most commonly used mobility-control methods are the water-alternating-gas (WAG) injection[5] and the application of foaming agents.[6] The WAG process can effectively reduce the relative permeability of a gas phase (e.g., CO_2) and its mobility. However, an excessive amount of the injected water in an oil reservoir can cause severe gravity segregation (i.e., water underlying and CO_2 overriding) and high water-cut. In addition, the so-called water blocking or shielding may seriously hinder oil recovery and finally result in a high residual oil saturation.[7] On the other hand, the foam lamellae in porous media can provide some effective resistance to the gas phase flow. In practice, nevertheless, how to properly generate foam and control its propagation in an oil formation under the actual reservoir conditions have always been challenging technical issues.[8]

In comparison with the above-mentioned two conventional mobility-control methods, thickening CO_2 by using a polymer as a direct thickener offers several distinct advantages. First, the water-blocking effect will be eliminated. Without water injection and the associated water production and treatment, the oil recovery will be more efficient, and the overall project will be more economical. Second, the CO_2−polymer mixture is rather stable under the actual reservoir conditions.[9] Third, the sweep efficiency of polymer-thickened CO_2 can be considerably improved due to a favorable mobility ratio, and its breakthrough can be significantly delayed. Hence, the ultimate oil recovery can be increased, and some field operational problems, such as severe CO_2 corrosion and excessive water production and treatment, can also be minimized.

Previous research work in thickening CO_2 has mainly focused on the identification of an appropriate polymer, which can be used as a thickener to effectively viscosify CO_2. Heller and coworkers measured the solubilities of 53 commercially available polymers in CO_2 and identified a total of 17 polymers that are soluble in CO_2.[10] In particular, poly(1-decene) (P-1-D) with a low molecular weight has the highest solubility in CO_2 and thus may be the best candidate for thickening CO_2. They also successfully synthesized α-olefin polymer, which is soluble in dense CO_2.[11] Bae and Irani found that supercritical CO_2 can also be substantially thickened or viscosified by using some silicon-based polymers together with an organic cosolvent.[12] The specific effects of different cosolvents on the solubilities of the silicone polymers in CO_2 were studied as well.[9] McHugh and coworkers reported that many fluorinated polymers are highly

Special Issue: John M. Prausnitz Festschrift

Received: October 15, 2010
Accepted: March 2, 2011
Published: March 18, 2011

CO_2-philic under high-temperature and high-pressure conditions.[13] Furthermore, a research team led by Drs. Enick and Beckman at the University of Pittsburgh studied fluoroacrylate−styrene copolymers and showed that they have adequate solubilities in pure CO_2 and can increase its viscosity by a factor of 6 to 8.[14,15] The temperature effect on the viscosity of fluorous polymer-thickened CO_2 was also examined.[16] However, the fluorous polymers are not suitable for viscosifying CO_2 in the oilfield applications because they are expensive and can cause some serious environmental issues. The molecular design of nonfluorous polymers for thickening CO_2 was initiated in 1999. It was found that the addition of a side chain with oxygen-containing groups (e.g., the carbonyl group) can increase the solubility of certain silicone oligomers in CO_2[17] and that a series of poly(ether carbonate) copolymers synthesized by using propylene and CO_2 can be readily dissolved into CO_2 at relatively low pressures.[18] Other oxygen-containing polymers with CO_2-philic compounds, such as poly(vinyl ethyl ether) (PVEE),[19] poly(vinyl acetate) (PVAc),[20] and amorphous poly(lactic acid) (PLA),[21] were also developed to enhance polymer solubility in supercritical CO_2 and thus increase its viscosity.

It is well-known that during CO_2 flooding, the oil−CO_2 two-phase flow is largely controlled by their interfacial interactions, such as the interfacial tension (IFT).[22] However, no experimental tests were conducted to study the effect of a polymer or thickener dissolved into CO_2 phase on the equilibrium IFT of a crude oil−polymer-thickened CO_2 system. Also, there were only a few coreflood tests with CO_2 thickened by using a polymer, in which a cosolvent was used to increase solubility of the polymer into CO_2.[9,12] At present, it remains unknown whether polymer-thickened CO_2 can effectively mobilize and even produce the residual oil after the complete or partial pure CO_2 flooding. In practice, it is still difficult to properly choose and accurately evaluate a candidate polymer as a direct thickener for CO_2. In principle, such a polymer should not only have an adequate solubility in CO_2 but also significantly viscosify CO_2 under the actual reservoir conditions.

In this paper, on the basis of the existing polymer-in-CO_2 solubility data reported in the literature, two commercially available low molecular weight polymers, PVEE and P-1-D, are chosen and tested as direct thickeners for CO_2. First, their cloud-point pressures in a range of possible reservoir pressures are measured at different known polymer solubilities in supercritical CO_2 by using a see-through windowed high-pressure cell. Then the equilibrium IFTs between a light crude oil and polymer-thickened CO_2 at different equilibrium pressures are measured by applying the axisymmetric drop shape analysis (ADSA) technique for the pendent drop case.[23] Third, the viscosities of thickened CO_2 with different known polymer solubilities at different pressures are measured by using a capillary viscometer. Lastly, a total of six high-pressure CO_2 coreflood tests are conducted under the so-called miscible conditions by using tight sandstone reservoir core plugs and reservoir oil and brine samples to examine the specific effect of each thickener on CO_2 improved or enhanced oil recovery. All of the experimental data for polymer-thickened CO_2 are compared with those for pure CO_2.

EXPERIMENTAL SECTION

Materials. In this study, two low molecular weight liquid polymers were purchased from Sigma-Aldrich Corporation:

Table 1. Compositional Analysis Results of Joffre Viking Original Light Crude Oil with the Asphaltene Content of w_{asp} = 0.0010 in Mass Fraction (Pentane Insoluble)

C_n	mass fraction	C_n	mass fraction	C_n	mass fraction
C_1	0.0000	C_{18}	0.0300	C_{35}	0.0101
C_2	0.0000	C_{19}	0.0233	C_{36}	0.0077
C_3	0.0000	C_{20}	0.0200	C_{37}	0.0077
C_4	0.0000	C_{21}	0.0231	C_{38}	0.0055
C_5	0.0110	C_{22}	0.0147	C_{39}	0.0081
C_6	0.0190	C_{23}	0.0189	C_{40}	0.0056
C_7	0.0633	C_{24}	0.0143	C_{41}	0.0056
C_8	0.0667	C_{25}	0.0171	C_{42}	0.0056
C_9	0.0550	C_{26}	0.0146	C_{43}	0.0063
C_{10}	0.0600	C_{27}	0.0141	C_{44}	0.0041
C_{11}	0.0483	C_{28}	0.0141	C_{45}	0.0041
C_{12}	0.0433	C_{29}	0.0120	C_{46}	0.0041
C_{13}	0.0408	C_{30}	0.0105	C_{47}	0.0037
C_{14}	0.0358	C_{31}	0.0116	C_{48}	0.0037
C_{15}	0.0383	C_{32}	0.0105	C_{49}	0.0037
C_{16}	0.0300	C_{33}	0.0073	C_{50+}	0.1108
C_{17}	0.0283	C_{34}	0.0077	Total	1.0000

Table 2. Physical and Chemical Properties of the Cleaned Reservoir Brine at P = 0.1 MPa

T/K	288.15	293.15	313.15
$\rho_{brine}/(g\cdot cm^{-3})$	1.012	1.011	1.005
$\mu_{brine}/(mPa\cdot s)$	1.19	1.03	0.67
pH at 293.15 K	8.23		
specific conductivity/($\mu S\cdot cm^{-1}$)	19 400		
refractive index at 298.15 K	1.3353		
chloride/($mg\cdot L^{-1}$)	4400		
sulfate/($mg\cdot L^{-1}$)	6.5		
total dissolved solids/($mg\cdot L^{-1}$)	13 900 at 453.15 K		
potassium/($mg\cdot L^{-1}$)	92		
sodium/($mg\cdot L^{-1}$)	5200		
calcium/($mg\cdot L^{-1}$)	20		
magnesium/($mg\cdot L^{-1}$)	77		
iron/($mg\cdot L^{-1}$)	0.012		
manganese/($mg\cdot L^{-1}$)	< 0.001		
barium/($mg\cdot L^{-1}$)	6.5		

PVEE, $[CH_2CH(OC_2H_5)]_n$, M_w = 3800 $g\cdot mol^{-1}$ and ρ = 0.968 $g\cdot cm^{-3}$ at 298.15 K; and P-1-D, $[CH_2CH[(CH_2)_7CH_3]]_n$, M_w = 910 $g\cdot mol^{-1}$ and ρ = 0.833 $g\cdot cm^{-3}$ at 298.15 K. They were used as direct thickeners to thicken or viscosify pure CO_2. The mole fraction purity of carbon dioxide (Praxair, Canada) used in this study was 0.99998. The CMG WinProp module (Version 2008.10, Computer Modeling Group Limited) was used to predict the densities of pure CO_2 with Peng−Robinson equation of state (EOS)[24] and its viscosities at different pressures and temperatures of interest.

The original light crude oil sample was collected from the Joffre Viking Pool in Alberta, Canada, with the reservoir temperature of T_{res} = 329.15 K. The density of the cleaned dead light crude oil sample was ρ_{oil} = 0.815 $g\cdot cm^{-3}$; the oil viscosity was μ_{oil} = 1.0 mPa·s at the atmospheric pressure and 329.15 K, and

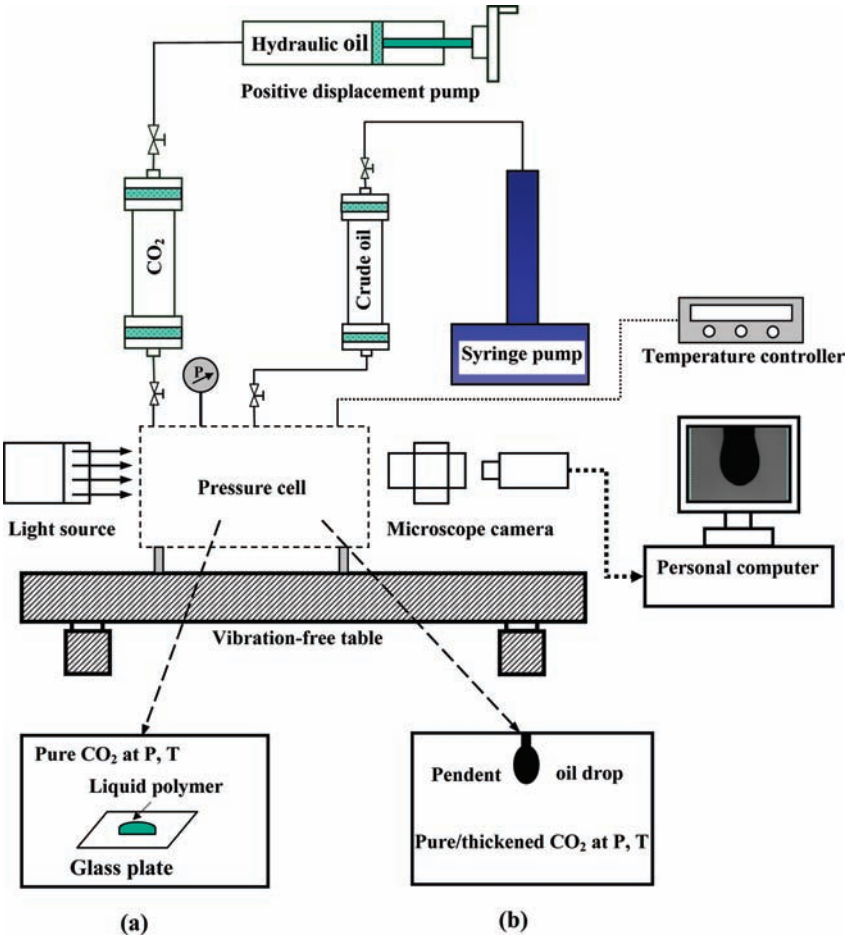

Figure 1. Schematic diagram of the experimental setup used for measuring (a) the polymer cloud-point pressure in pure CO_2 and (b) the equilibrium interfacial tension (IFT) between the light crude oil and the pure/polymer-thickened CO_2 by applying the axisymmetric drop shape analysis (ADSA) technique for the pendent drop case.

the mass fraction of its asphaltene content (pentane insoluble) was w_{asp} = 0.0010. The compositional analysis result of the cleaned dead light crude oil sample was obtained by using the standard ASTM D86[25] and is given in Table 1. It can be seen from the table that there are no hydrocarbon components under C_4 and that the mass fraction of the heavy hydrocarbon components (i.e., C_{50+}) is equal to $w(C_{50+})$ = 0.1108. A reservoir brine sample was taken from the same pool, cleaned by rinsing it through paper filters, and analyzed in the laboratory. Its detailed physical and chemical properties are listed in Table 2. A number of tight sandstone reservoir core plugs were collected from several wells located in the Joffre Viking Pool at the reservoir depths of (1516 to 1521) m.

Polymer Cloud-Point Pressure Measurement. In the literature, a windowed high-pressure cell with a variable volume was used to measure the polymer cloud-point pressure at a known polymer solubility in pure CO_2.[26] In this study, a visual method was applied, and a schematic diagram of the experimental setup used to measure the cloud-point pressure of either polymer in pure CO_2 at a known polymer solubility is shown in Figure 1. The major component of this experimental setup was a see-through windowed high-pressure cell (IFT-10, Temco) with a net volume of 49.5 cm^3, which is shown in Figure 1a for the polymer cloud-point pressure measurement. A light source and a glass diffuser (240-341, Dyna-Lume) were placed on the left-hand side of the high-pressure cell to provide sufficient and uniform illumination for polymer-thickened CO_2. A monochrome microscope camera (MZ6, Leica) was positioned on the right-hand side of the high-pressure cell to capture the digital image of polymer-thickened CO_2 inside the pressure cell at any time. The digital image of thickened CO_2 under each different equilibrium pressure was acquired in a tagged image file (TIF) format by using a digital frame grabber (Ultra II, Coreco Imaging) and stored in a Dell desktop computer. A numeric reading (0 to 255) of light intensity is available at each pixel or point of such an acquired monochrome digital image of polymer-thickened CO_2.

Prior to each polymer cloud-point pressure measurement, the see-through windowed high-pressure cell shown in Figure 1a was cleaned with kerosene and then dried with nitrogen. First, a small known amount of either liquid polymer (i.e., PVEE or P-1-D) was slowly poured and gently placed onto a small glass plate, which was horizontally positioned inside the high-pressure cell. Then the pressure cell was closed, sealed, and flushed with pure CO_2. The high-pressure cell was wrapped with a heating tape (HT95504X1, Electrothermal), preheated to and maintained at the actual reservoir temperature of T_{res} = 329.15 K by using a temperature controller (3PN1010B, Staco) with the accuracy of 0.1 K. Afterward, pure CO_2 was slowly introduced into the high-pressure cell to increase its pressure by 0.2 MPa each step at a

time interval of 20 min. It was found by trial and error that this time interval was long enough for the CO_2−polymer system to reach an equilibrium state, which was indicated by a constant equilibrium pressure. The equilibrium pressure was accurately measured by using a digital precision test gauge (type 2089, Ashcroft) with the accuracy of 0.05 %. This pressurization process was continued until the liquid polymer was completely dissolved into CO_2 at a sufficiently high pressure. Hence, a clear transparent single phase (i.e., CO_2 solution with dissolved polymer) was formed inside the high-pressure cell. Finally, the test pressure was reduced by 0.2 MPa each step at the same time interval until polymer-thickened CO_2 or CO_2 solution became cloudy and the so-called polymer cloud-point state was reached. The corresponding test pressure was termed the cloud-point pressure of this polymer in pure CO_2 at the known polymer solubility and the actual reservoir temperature. For each CO_2−polymer system, the polymer cloud-point pressure was measured twice and found to be within 0.2 MPa. The above-described polymer cloud-point pressure measurement procedure was repeated with a different known amount of the same liquid polymer at the beginning until enough polymer cloud-point pressure versus its solubility data points at T_{res} = 329.15 K were obtained.

More specifically, after a small known amount of either liquid polymer (i.e., PVEE or P-1-D) was completely dissolved into supercritical CO_2 at a sufficiently high pressure, CO_2 and polymer became one phase, and thus CO_2 solution was clear and transparent. For example, a transparent P-1-D-thickened CO_2 phase was found at 20.9 MPa and 329.15 K, and its digital image was acquired by using the microscope camera. The corresponding digital photograph was taken by using a Nikon digital camera (Coolpix 5700, Nikon, Japan) to depict the appearance of the entire high-pressure cell filled with CO_2 solution. In this case, the transmitted light intensity ranging from 0 (black) to 255 (white) at every pixel of the acquired monochrome digital image of CO_2 solution reached a maximum value close to 250. An average value of the numeric readings of light intensity at 25 (i.e., 5 rows × 5 columns) representative pixels or points was obtained and used as a maximum reference value at a later time. Then the test pressure was reduced by 0.2 MPa each step at a time interval of 20 min until the polymer cloud-point state was reached. For instance, the cloud-point state at P_{cp} = 20.1 MPa and T_{res} = 329.15 K was determined from the digital image of P-1-D-thickened CO_2 acquired by using the microscope camera and further verified with the corresponding digital photograph taken by using the Nikon digital camera. The cloud-point state for P-1-D-thickened CO_2 was assumedly achieved when the average value of the numeric readings of light intensity at the same 25 representative pixels was about 150 or 40 % lower than the maximum reference value at P = 20.9 MPa and T_{res} = 329.15 K. In the literature, a similar method was applied to determine the polymer cloud-point pressure, P_{cp}, though 90 % reduction in transmitted light intensity of the polymer-thickened CO_2 or CO_2 solution was used elsewhere.[13]

Equilibrium IFT Measurement. In this study, the same high-pressure setup in Figure 1 used for measuring the polymer cloud-point pressure in pure CO_2 was also used to measure the equilibrium IFT between the light crude oil and pure/thickened CO_2 by applying the axisymmetric drop shape analysis (ADSA) technique for the pendent drop case. The see-through windowed high-pressure cell used for the equilibrium IFT measurement is shown in Figure 1b. The entire ADSA system and high-pressure cell were placed on a vibration-free table (RS4000, Newport). A stainless steel syringe needle was installed at the top of the pressure cell and used to form a pendent oil drop. The light crude oil was introduced from the original light crude oil sample cylinder (500-10-P-316-2, DBR) to the syringe needle by using a programmable syringe pump (100DX, ISCO Inc.). The light source and the glass diffuser were used to provide sufficient and uniform illumination for the pendent oil drop surrounded by pure or polymer-thickened CO_2. The microscope camera was used to capture the digital image of the dynamic pendent oil drop inside the pressure cell at any time.

Prior to each IFT measurement, the high-pressure cell was first cleaned with kerosene and then flushed with nitrogen and pure CO_2, respectively. To measure the IFT of the light crude oil−pure CO_2 system, the pressure cell was pressurized with pure CO_2 to a prespecified pressure at T_{res} = 329.15 K. After the pressure and temperature inside the pressure cell reached their stable values, the crude oil was introduced from the original light crude oil sample cylinder to the high-pressure cell to form a pendent oil drop at the tip of the syringe needle. Once a well-shaped pendent oil drop was formed and surrounded by pure CO_2, the sequential digital images of the dynamic pendent oil drop at different times were acquired and stored automatically in the personal computer. To measure the IFT of the light crude oil−polymer-thickened CO_2 system, a sufficient amount (i.e., 0.6 g) of either liquid polymer was gently poured and placed onto the small glass plate at the beginning to ensure that the polymer solubility in CO_2 at any equilibrium pressure in the range of P_{eq} = (8.1 to 12.5) MPa was reached. Afterward, the high-pressure cell was pressurized with pure CO_2 to a prespecified pressure at T_{res} = 329.15 K. A period of 20 min was allowed so that there was no further dissolution of the polymer into CO_2, and the polymer solubility in CO_2 at each equilibrium pressure was achieved. After the pressure and temperature inside the high-pressure cell reached their stable values, the same procedure for measuring the light crude oil−pure CO_2 IFT was followed. Finally, the ADSA program for the pendent drop case was executed to analyze the digital images of the dynamic pendent oil drop and determine the dynamic IFTs of the light crude oil−pure or polymer-thickened CO_2 system at different equilibrium pressures. The dynamic IFT measurement was repeated for at least three different pendent oil drops to ensure satisfactory repeatability at each equilibrium pressure and T_{res} = 329.15 K. Only the average value of the equilibrium IFTs of three repeated IFT measurements at each equilibrium pressure and T_{res} = 329.15 K was noted and is presented in this paper. The overall accuracy of the measured equilibrium IFTs is equal to 0.05 $mJ \cdot m^{-2}$.

Polymer-Thickened CO_2 Viscosity Measurement. To accurately measure the viscosity of polymer-thickened CO_2 at each reservoir pressure and T_{res} = 329.15 K, a house-made capillary viscometer was constructed, and its schematic diagram is shown in Figure 2. A 40 ft long stainless steel tubing (SS-T1-S-020-6ME, Swagelok) was coiled onto two cylinders. This capillary tubing has the following nominal dimensions: an outer diameter (OD) of 1/16 in. and a wall thickness of 0.02 in. This long and small capillary tubing was chosen to ensure that a pressure drop along it was large enough to accurately measure the polymer-thickened CO_2 viscosity. An automatic displacement pump (PMP-1000-1-10-MB, DBR, Canada) was used to inject thickened CO_2 from its sample cylinder into the capillary tubing. A back-pressure regulator (BPR) (BPR 50, Temco, USA) was used to maintain the outlet pressure of the long capillary tubing during the visco-

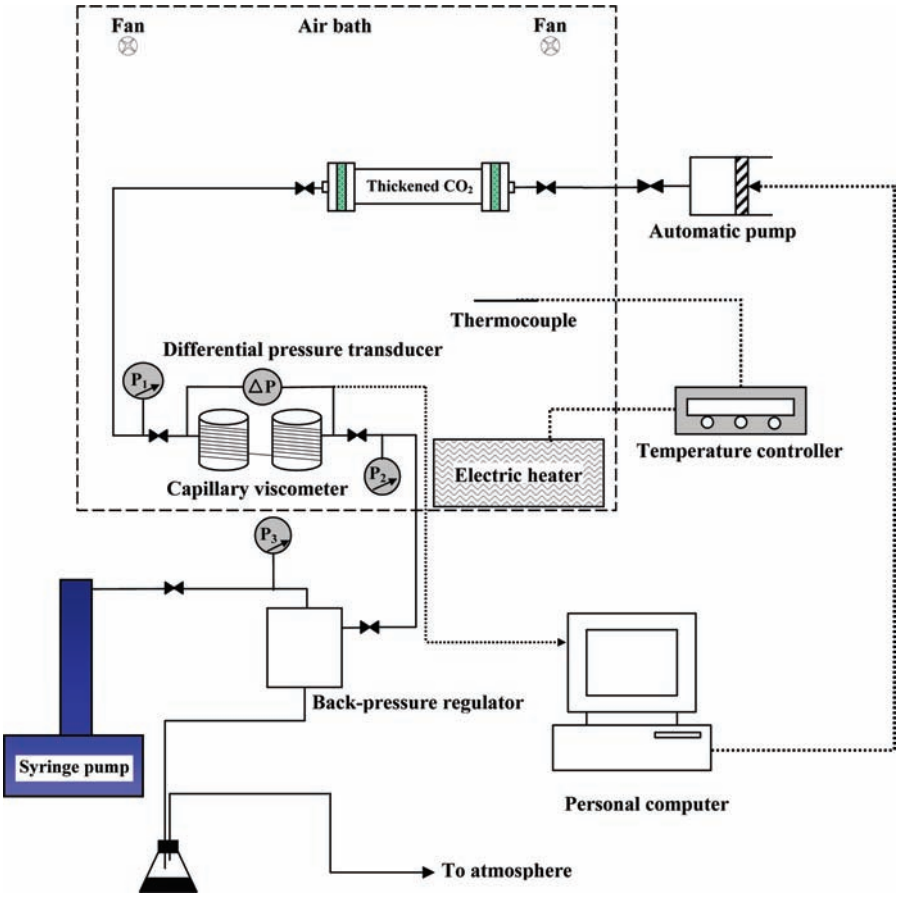

Figure 2. Schematic diagram of a capillary viscometer used for measuring the viscosity of thickened CO_2 by using a polymer as a direct thickener.

sity measurement. The pressure drop along the tubing was measured by using a differential pressure transducer (P55D, Validyne, USA). The measured differential pressure data were stored automatically in a personal computer at a preset time interval. The capillary viscometer and thickened CO_2 sample cylinder were placed inside an air bath. An electric heater (HZ-315C, Super Electric Co., Canada) and a temperature controller (Standard-89000-00, Cole−Parmer) were used to heat the air bath and keep it at a constant temperature. Moreover, distilled water with μ_w = 0.979 mPa·s at T = 294.15 K was used as a standard viscosity liquid and injected through the capillary tubing at different injection rates of (0.5 to 15.0) $cm^3 \cdot min^{-1}$ to validate the capillary viscometer. Then the Poiseuille equation was applied to determine the so-called "effective radius" of the capillary tubing.

Prior to each polymer-thickened CO_2 viscosity measurement, the capillary tubing was cleaned with toluene and then flushed with nitrogen to ensure that there was not any leftover polymer trace from the previous viscosity measurement. Then it was vacuumed, and the BPR was set at a prespecified test pressure. The capillary viscometer and thickened CO_2 sample cylinder were placed inside the air bath, which was heated to and maintained at T_{res} = 329.15 K. The polymer-thickened CO_2 inside the sample cylinder was pressurized and injected into the capillary tubing by using the automatic displacement pump. After the differential pressure reached a stable value, it was measured by using the differential pressure transducer. The polymer-thickened CO_2 viscosity measurements were carried out at three different injection rates of (0.1, 0.3, and 0.5) $cm^3 \cdot min^{-1}$, respectively. The Reynolds numbers at the three injection rates and all of the test pressures were calculated to be less than 75 so that there was a laminar flow in each polymer-thickened CO_2 viscosity measurement. Then the Poiseuille equation was applied to determine the polymer-thickened CO_2 viscosity at each injection rate. It was found that the measured polymer-thickened CO_2 viscosity remained virtually the same at each test pressure, irrespective of the three different injection rates used. This fact shows that the thickened CO_2 with low polymer solubilities tested in this study behaves as a Newtonian fluid.[12]

Polymer-Thickened CO_2 Coreflood Test. A schematic diagram of the high-pressure coreflood apparatus used in pure or thickened CO_2 coreflood tests is shown in Figure 3. Prior to each CO_2 coreflood test, three new sandstone reservoir core plugs were placed in series inside the Dean−Stark extractor (09-556D, Fisher Scientific) and thoroughly cleaned with toluene, methanol, and chloroform in sequence to remove hydrocarbons, salts, and clays, respectively. The automatic displacement pump was used to displace the light crude oil, reservoir brine, pure or thickened CO_2 in sequence through the composite reservoir core plugs in series inside a coreholder (RCHR-2.0, Temco). The tap water was pumped by using a manual displacement pump (HAT-250-100, Temco) to apply an overburden pressure, which was always maintained at 3 MPa higher than the inlet pressure of the coreholder. The composite reservoir core plugs used in the six coreflood tests were (8.43 to 8.74) in. long and 2.00 in. in diameter. Five high-

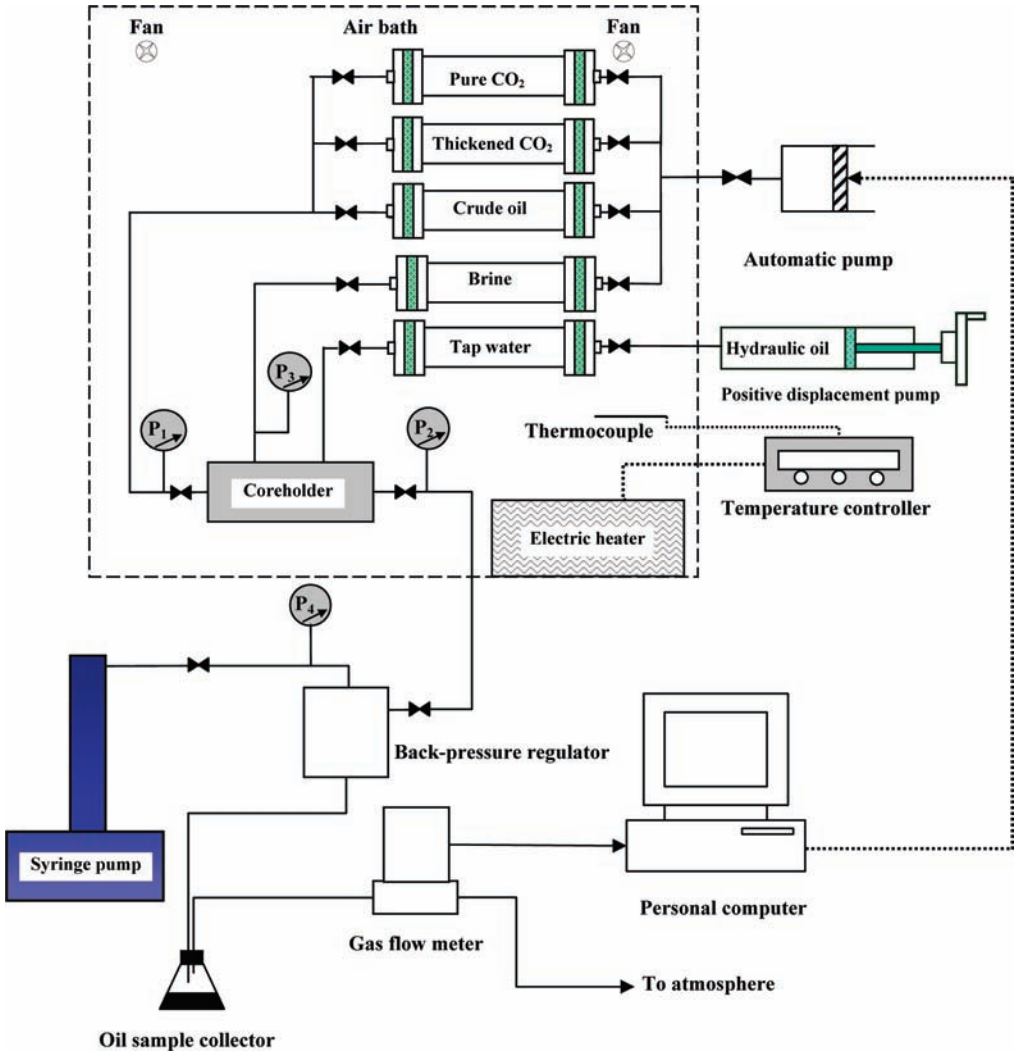

Figure 3. Schematic diagram of the high-pressure CO_2 coreflood apparatus.

pressure sample cylinders were used to store and deliver the light crude oil, reservoir brine, pure CO_2, thickened CO_2, and tap water, respectively. The entire high-pressure CO_2 coreflood apparatus and five fluid sample cylinders were placed inside the air bath. The electric heater and the temperature controller were used to heat the air bath and keep its constant temperature of T_{res} = 329.15 K. The back-pressure regulator at the coreholder outlet was used to maintain a prespecified injection pressure (i.e., 15.2 MPa for PVEE or 16.2 MPa for P-1-D) inside the coreholder during each CO_2 flooding test. The cumulative produced oil volume inside a graduated cylinder was automatically recorded by using a digital video camera (Logitech Webcam C200, China). A gas flow meter (GFM 17, Aalborg) was used to automatically measure the cumulative produced gas volume. It should be noted that there was no brine production in any CO_2 coreflood test conducted in this study.

The general procedure for preparing each CO_2 coreflood test is briefly described as follows. After the three sandstone reservoir core plugs were cleaned and dried, they were assembled in series in the horizontal coreholder and vacuumed for 48 h. Then the cleaned reservoir brine was imbibed to measure the porosity of the composite reservoir core plugs. Afterward, the cleaned reservoir brine was injected at three to five different flow rates, q_{brine} = (0.1 to 0.5) $cm^3 \cdot min^{-1}$, to measure the absolute permeability of the composite reservoir core plugs.

For coreflood Test 1 with PVEE and Test 4 with P-1-D, pure CO_2 flooding was conducted and then followed by the subsequent polymer-thickened CO_2 flooding. First, the original light crude oil was injected at q_{oil} = 0.1 $cm^3 \cdot min^{-1}$ to displace the reservoir brine at 329.15 K until the so-called connate water saturation was achieved. Then a total of 3.00 pore volume (P.V.) of the original light crude oil was further injected to pressurize the core plugs until the prespecified coreflood test pressure was reached. Afterward, pure CO_2 was injected at the injection rate of q_{CO_2} = 0.4 $cm^3 \cdot min^{-1}$ to produce the light crude oil from the coreholder until a total of 2.00 P.V. of pure CO_2 was injected and no more oil was produced. It was found that the pure CO_2 breakthrough always occurred when approximately 0.50 P.V. of pure CO_2 was injected. The subsequent polymer-thickened CO_2 flooding commenced after the complete pure CO_2 flooding at the same injection rate of $q_{sol.}$ = 0.4 $cm^3 \cdot min^{-1}$ and terminated after a total of 2.00 P.V. of thickened CO_2 was injected and no more oil was produced.

For coreflood Test 2 with PVEE and Test 5 with P-1-D, pure CO_2 flooding was conducted until the pure CO_2 breakthrough

Table 3. Polymer Solubility in CO_2 in Mass Fraction, $\chi_{sol.}$, Measured Polymer Cloud-Point Pressure, P_{cp}, Thickened and Pure CO_2 Viscosities, $\mu_{sol.}$ and μ_{CO_2}, and Their Ratios, $\mu_{sol.}/\mu_{CO_2}$, at T_{res} = 329.15 K

polymer	$\chi_{sol.}$	P_{cp} / MPa	$\mu_{sol.}$ / mPa·s	μ_{CO_2} / mPa·s	$\mu_{sol.}/\mu_{CO_2}$
PVEE[a]	0.0067	14.6	0.68	0.048	14.17
	0.0069	16.1	0.78	0.053	14.72
	0.0073	17.1	0.85	0.056	15.18
	0.0077	18.3	0.89	0.059	15.08
	0.0080	19.7	0.95	0.063	15.08
P-1-D[b]	0.0056	14.7	0.70	0.049	14.29
	0.0061	15.2	0.77	0.051	15.10
	0.0066	17.0	0.83	0.056	14.82
	0.0070	18.5	0.87	0.060	14.50
	0.0081	20.1	0.93	0.064	14.53

[a] PVEE: poly(vinyl ethyl ether). [b] P-1-D: poly(1-decene).

occurred, and then polymer-thickened CO_2 was injected as an alternate solvent. Pure CO_2 injection at q_{CO_2} = 0.4 $cm^3 \cdot min^{-1}$ was terminated after the pure CO_2 breakthrough occurred at 0.46 injected P.V. for Test 2 or 0.47 injected P.V. for Test 5. The subsequent polymer-thickened CO_2 flooding commenced after the partial pure CO_2 flooding at the same injection rate of $q_{sol.}$ = 0.4 $cm^3 \cdot min^{-1}$ and terminated after a total of 2.00 P.V. of thickened CO_2 was injected and no more oil was produced.

For coreflood Test 3 with PVEE and Test 6 with P-1-D, polymer-thickened CO_2 was injected at the injection rate of $q_{sol.}$ = 0.4 $cm^3 \cdot min^{-1}$ for the so-called secondary oil recovery. There was no pure CO_2 flooding in these two tests. The thickened CO_2 breakthrough occurred at 0.69 injected P.V. for Test 3 with PVEE or 0.80 injected P.V. for Test 6 with P-1-D. Polymer-thickened CO_2 flooding was stopped after a total of 2.00 P.V. of thickened CO_2 was injected and no more oil was produced.

RESULTS AND DISCUSSION

Polymer Cloud-Point Pressure. In this work, the polymer cloud-point pressure in supercritical CO_2 is measured in the following two pressure ranges at T_{res} = 329.15 K, P_{cp} = 14.6 to 19.7 MPa for PVEE and P_{cp} = 14.7 to 20.1 MPa for P-1-D. These two pressure ranges are chosen because future CO_2 EOR projects in the Joffre Viking Pool are expectedly operated at P_{res} = (14 to 20) MPa and T_{res} = 329.15 K.[3] After the polymer cloud-point pressure is measured, the polymer solubility in CO_2, $\chi_{sol.}$, at the cloud-point state (P_{cp} and T_{res} = 329.15 K) is determined from:

$$\chi_{sol.} = \frac{m_p/g}{m_p/g + (\rho_{CO_2}/g\cdot cm^{-3})\cdot\left(V_{cell}/cm^3 - \frac{m_p/g}{\rho_p/g\cdot cm^{-3}}\right)} \quad (1)$$

where m_p and ρ_p are the known mass and density of polymer to be dissolved into CO_2; ρ_{CO_2} is pure CO_2 density at P_{cp} and T_{res} = 329.15 K, which is calculated by using the CMG WinProp module; and V_{cell} is the volume of the high-pressure cell filled with CO_2, which is equal to 49.5 cm^3.

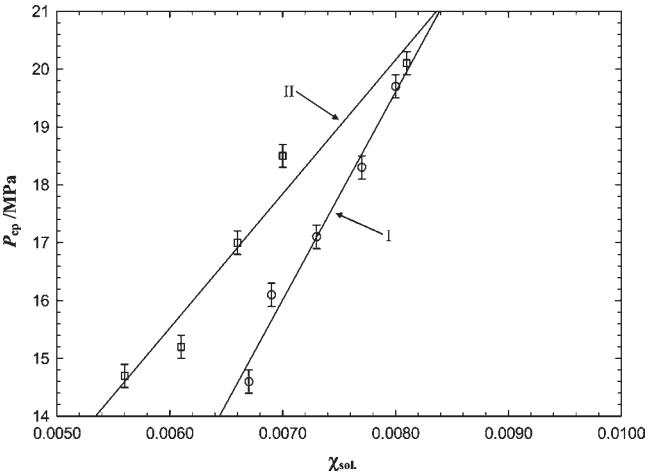

Figure 4. Measured polymer cloud-point pressures, P_{cp}, at different polymer solubilities in mass fraction, $\chi_{sol.}$, in pure CO_2 and T_{res} = 329.15 K. ○, PVEE; □, P-1-D. Line I is eq 2, and line II is eq 3.

The measured cloud-point pressures of two respective polymers in supercritical CO_2 at different known polymer solubilities and T_{res} = 329.15 K are given in Table 3 and further plotted in Figure 4. These measured polymer cloud-point pressure versus solubility data show that both polymers can be adequately dissolved into CO_2 at their cloud-point pressures tested and T_{res} = 329.15 K. In general, PVEE has a much higher solubility than P-1-D at the same and low polymer cloud-point pressure. This is because PVEE has an oxygen-containing ether group in the backbone of its molecular structure, whereas P-1-D is a typical hydrocarbon polymer with no oxygen component. It has already been proven that the oxygen-containing ether group is CO_2-philic and thus enhances the solubility of a hydrocarbon polymer in dense CO_2 if the ether group is attached to its backbone, such as PVEE.[20] With the measured polymer cloud-point pressure versus solubility data, as a first approximation, P_{cp} is linearly correlated to $\chi_{sol.}$ by applying the linear regression:

$$P_{cp}/MPa = 3590.753\chi_{sol.} - 9.124 \text{ for PVEE } (0.0067 \le \chi_{sol.} \le 0.0080, R^2 = 0.976) \quad (2)$$

$$P_{cp}/MPa = 2318.082\chi_{sol.} + 1.615 \text{ for P-1-D } (0.0056 \le \chi_{sol.} \le 0.0081, R^2 = 0.958) \quad (3)$$

Equilibrium IFT between the Light Crude Oil and Pure/Polymer-Thickened CO_2. In this study, the equilibrium IFTs between the light crude oil and the pure/polymer-thickened CO_2 are measured at T_{res} = 329.15 K in the equilibrium pressure ranges of P_{eq} = (9.1 to 13.6) MPa for pure CO_2, (8.1 to 10.3) MPa for PVEE-thickened CO_2, and (8.7 to 12.5) MPa for P-1-D-thickened CO_2. The polymer-thickened CO_2 density, $\rho_{sol.}$, can be calculated from:

$$\rho_{sol.}/g\cdot cm^{-3} = \frac{m_p/g + (\rho_{CO_2}/g\cdot cm^{-3})\cdot\left(V_{cell}/cm^3 - \frac{m_p/g}{\rho_p/g\cdot cm^{-3}}\right)}{V_{cell}/cm^3} \quad (4)$$

dx.doi.org/10.1021/je1010449 |J. Chem. Eng. Data 2011, 56, 1069–1079

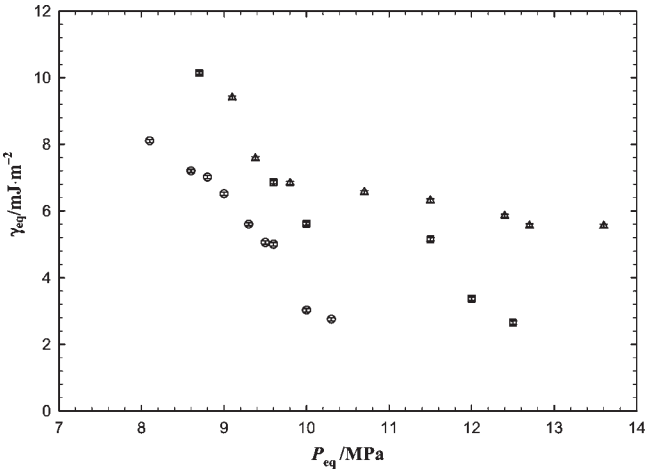

Figure 5. Measured equilibrium IFTs, γ_{eq}, of the light crude oil−pure/thickened CO_2 systems at different equilibrium pressures, P_{eq}, and T_{res} = 329.15 K. △, pure CO_2; ○, PVEE-thickened CO_2; □, P-1-D-thickened CO_2.

The measured equilibrium IFTs of three light crude oil−pure/polymer-thickened CO_2 systems at different equilibrium pressures and T_{res} = 329.15 K are plotted in Figure 5. It should be noted that when the equilibrium pressure is higher than certain value, the dynamic pendent oil drop cannot stay at the tip of the syringe needle long enough for the equilibrium IFT measurement to be completed.

In comparison of the measured equilibrium IFTs between the light crude oil and polymer-thickened CO_2 and those between the light crude oil and pure CO_2, it becomes obvious from Figure 5 that PVEE can significantly reduce the IFT between the light crude oil and the polymer-thickened CO_2 at any equilibrium pressures tested. Although the IFTs for P-1-D-thickened CO_2 at pressures lower than 10 MPa are close to those for pure CO_2, the polymer-thickened CO_2 leads to significant IFT reduction at higher equilibrium pressures. This polymer-induced equilibrium IFT reduction at a high equilibrium pressure is attributed to the following two possible reasons. First, dissolution of each hydrocarbon polymer into pure CO_2 may considerably increase the solubility of the polymer-thickened CO_2 in a light crude oil with a large amount of light and intermediate hydrocarbons as polymer-thickened CO_2 and the light crude oil become more alike, in comparison with pure CO_2 and the light crude oil. As shown in Figure 4, PVEE has a much higher solubility in pure CO_2 than P-1-D at the same polymer cloud-point pressure. This is why the measured equilibrium IFTs for PVEE-thickened CO_2 are much lower than those for P-1-D-thickened CO_2. Second, as given in eq 4, polymer-thickened CO_2 has a slightly higher density than pure CO_2 so that its density difference with the light crude oil is smaller, and thus their IFT is lower.[27] It is expected that the reduced equilibrium IFT between the light crude oil and the polymer-thickened CO_2 will enhance their miscibility and help to mobilize and produce the residual oil from a light oil reservoir after it is flooded with pure CO_2.

Polymer-Thickened CO_2 Viscosity. In this study, the Poiseuille equation is applied to determine polymer-thickened CO_2 (i.e., CO_2 solution) viscosity $\mu_{sol.}$:[9]

$$\mu_{sol.}/\text{mPa}\cdot\text{s} = \frac{\pi(r_{eff}/\text{m})^4\cdot(\Delta P/\text{mPa})}{8(Q/\text{m}^3\cdot\text{s}^{-1})\cdot(L/\text{m})} \quad (5)$$

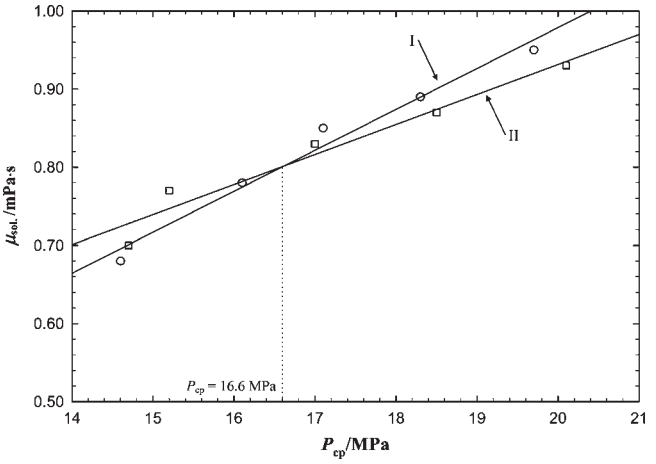

Figure 6. Measured polymer-thickened CO_2 viscosities, μ_{sol}, at different polymer cloud-point pressures, P_{cp}, and T_{res} = 329.15 K. ○, PVEE-thickened CO_2; □, P-1-D-thickened CO_2. Line I is eq 7, and line II is eq 8.

where ΔP and Q are the measured pressure drop and volume injection rate of polymer-thickened CO_2 through the capillary viscometer; r_{eff} and L are the effective radius and length of the capillary tubing. The corresponding shear rate at the wall of the tubing ε_w is equal to:[9]

$$\varepsilon_w/\text{s}^{-1} = \frac{4(Q/\text{m}^3\cdot\text{s}^{-1})}{\pi(r_{eff}/\text{m})^3} \quad (6)$$

The measured polymer-thickened CO_2 viscosities $\mu_{sol.}$ at different polymer cloud-point pressures or solubilities are listed and compared with pure CO_2 viscosities μ_{CO_2} in Table 3. The calculated corresponding wall shear rates at the three different injection rates of (0.1, 0.3, and 0.5) $\text{cm}^3\cdot\text{min}^{-1}$ are found to be (11.37, 34.11, and 56.85) s^{-1}, respectively. In general, it is found from the ratios of $\mu_{sol.}$ to μ_{CO_2} in Table 3 that PVEE- or P-1-D-thickened CO_2 viscosity $\mu_{sol.}$ is approximately (13 to 14) times higher than the pure CO_2 viscosity μ_{CO_2} at P_{cp} = (14.6 to 20.1) MPa and T_{res} = 329.15 K. Although the solubility of either polymer in pure CO_2 is less than 0.01 in mass fraction, both polymers show strong abilities to viscosify pure CO_2.

To more accurately compare the effects of two polymers on thickened CO_2 viscosity, the measured viscosities of either polymer-thickened CO_2 at different polymer cloud-point pressures are further plotted in Figure 6. It is seen from this figure that, at P_{cp} < 16.6 MPa, P-1-D-thickened CO_2 has a marginally higher viscosity than PVEE-thickened CO_2. At P_{cp} > 16.6 MPa, nevertheless, PVEE-thickened CO_2 has a slightly higher viscosity than P-1-D-thickened CO_2. With the measured polymer-thickened CO_2 viscosity versus polymer cloud-point pressure data, $\mu_{sol.}$ is linearly correlated to P_{cp} by applying the linear regression:

$$\mu_{sol.}/\text{mPa}\cdot\text{s} = 0.052(P_{cp}/\text{MPa}) - 0.070 \text{ for PVEE } (14.6 \le P_{cp}/\text{MPa} \le 19.7, R^2 = 0.977) \quad (7)$$

$$\mu_{sol.}/\text{mPa}\cdot\text{s} = 0.038(P_{cp}/\text{MPa}) + 0.163 \text{ for P-1-D } (14.7 \le P_{cp}/\text{MPa} \le 20.1, R^2 = 0.951) \quad (8)$$

In addition, to compare each polymer's ability to viscosify pure CO_2 at the same polymer solubility, Figures 4 and 6 are combined

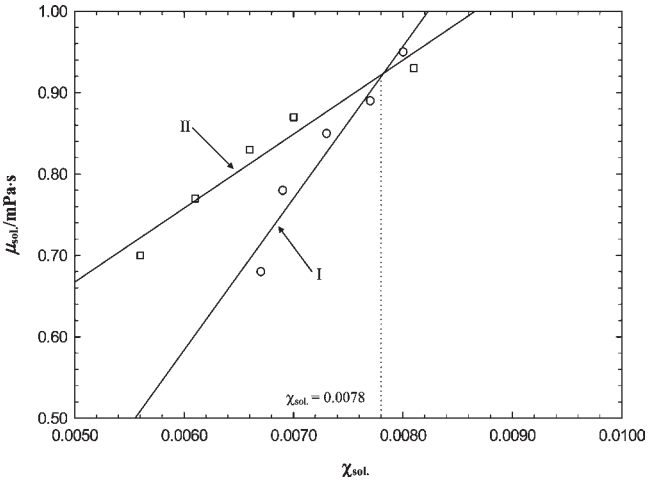

Figure 7. Measured polymer-thickened CO_2 viscosities, $\mu_{sol.}$, at different polymer solubilities in mass fraction, $\chi_{sol.}$, in pure CO_2 and T_{res} = 329.15 K. ○, PVEE-thickened CO_2; □, P-1-D-thickened CO_2. Line I is eq 9; and line II is eq 10.

Table 4. Physical Properties of the Composite Sandstone Reservoir Core Plugs, Coreflood Experimental Conditions, and Oil Recovery Factors at T_{res} = 329.15 K[a]

test no.	polymer	ϕ %	k mD	S_{oi} %	S_{wc} %	P MPa	RF_{CO_2} %	$RF_{sol.}$ %	RF_{total} %
1	PVEE[b]	13.90	3.0	37.80	62.20	15.2	69.60	2.20	71.80
2	PVEE	14.54	8.9	33.56	66.44	15.2	46.11	33.60	79.71
3	PVEE	16.70	7.3	32.80	67.20	15.2	—	72.96	72.96
4	P-1-D[c]	14.29	3.5	38.07	61.93	16.2	71.73	0.00	71.73
5	P-1-D	14.59	5.5	35.94	64.06	16.2	47.05	32.84	79.89
6	P-1-D	15.21	5.6	36.35	63.65	16.2	—	82.00	82.00

[a] ϕ: porosity. k: absolute permeability. S_{oi}: initial oil saturation. S_{wc}: connate water saturation. P: test pressure. RF_{CO_2}: pure CO_2 oil recovery factor, i.e., the ratio of the volume of produced oil to that of the original oil-in-place (OOIP). $RF_{sol.}$: polymer-thickened CO_2 oil recovery. [b] PVEE: poly(vinyl ethyl ether). [c] P-1-D: poly(1-decene).

and replotted in Figure 7. It is clearly seen from this figure that, at the same polymer solubility, P-1-D-thickened CO_2 has a much higher viscosity than PVEE-thickened CO_2, especially at low polymer solubilities. At a high polymer solubility close to $\chi_{sol.}$ = 0.0078 in mass fraction, these two polymers show similar abilities to viscosify pure CO_2. This is because with the same repeated units of monomers, P-1-D has a longer chain size so that it has a much stronger ability to thicken pure CO_2. In summary, P-1-D may be a better CO_2 thickener if the reservoir pressure is high enough for it to achieve an adequate solubility in pure CO_2. With the measured polymer-thickened CO_2 viscosity versus polymer solubility data, $\mu_{sol.}$ is linearly correlated to $\chi_{sol.}$ by applying the linear regression:

$$\mu_{sol.}/\text{mPa·s} = 186.643\chi_{sol.} - 0.536 \text{ for PVEE } (0.0067 \le \chi_{sol.} \le 0.0080, R^2 = 0.938) \quad (9)$$

$$\mu_{sol.}/\text{mPa·s} = 90.960\chi_{sol.} + 0.212 \text{ for P-1-D } (0.0056 \le \chi_{sol.} \le 0.0081, R^2 = 0.950) \quad (10)$$

Polymer-Thickened CO_2 Oil Recovery. In this study, a total of six high-pressure CO_2 coreflood tests were carried out under the miscible flooding conditions, that is, the coreflood test pressure is higher than the so-called minimum miscibility pressure (MMP) of 12 MPa.[3] The physical properties of the composite sandstone reservoir core plugs, coreflood experimental conditions, and oil recovery factors for pure and/or polymer-thickened CO_2 flooding processes are listed in Table 4. The coreflood test pressures of P = 15.2 MPa for PVEE (Tests 1, 2, and 3) and P = 16.2 MPa for P-1-D (Tests 4, 5, and 6) are chosen so that these two polymers have close solubilities in pure CO_2 but different thickened CO_2 viscosities at these two respective test pressures. Figure 8a shows the measured total oil recovery factor versus injected pore volume (P.V.) of pure and polymer-thickened CO_2 (Test 1 with PVEE and Test 4 with P-1-D). The pure CO_2 breakthrough occurs at approximately 0.5 injected P.V. in these two tests, and the corresponding oil recovery factor is equal to 52.17 % for Test 1 or 54.40 % for Test 4. The oil recovery factor continues to increase gradually up to 69.60 % for Test 1 or 71.73 % for Test 4 at a total of 2.00 injected P.V. of pure CO_2 when no more oil is produced due to pure CO_2 flooding. In Test 1, the subsequent injection of PVEE-thickened CO_2 as an alternate solvent marginally mobilizes the residual oil left after the complete pure CO_2 flooding and further enhances oil recovery by 2.20 % of the OOIP, which is equivalent to 7.24 % of the residual-oil-in-place (ROIP). However, the subsequent injection of P-1-D-thickened CO_2 as an alternate solvent in Test 4 has no effect on the EOR.

In high-pressure coreflood Test 2 with PVEE and Test 5 with P-1-D, polymer-thickened CO_2 is injected immediately after the pure CO_2 breakthrough. The oil recovery factors of pure or polymer-thickened CO_2 flooding at different injected pore volumes are plotted in Figure 8b. The pure CO_2 breakthrough occurs at 0.46 injected P.V. for Test 2 or 0.47 injected P.V. for Test 5, and the corresponding oil recovery factor is equal to 46.11 % for Test 2 or 47.05 % for Test 5. The subsequent injection of PVEE-thickened CO_2 as an alternate solvent significantly mobilizes the residual oil left after the partial pure CO_2 flooding and further produces 33.60 % of the OOIP in Test 2. Similarly, the subsequent injection of P-1-D-thickened CO_2 as an alternate solvent further enhances 32.84 % of the OOIP in Test 5. The total oil recovery factor is equal to 79.71 % for Test 2 with PVEE or 79.89 % for Test 5 with P-1-D, which is considerably higher than 71.80 % for Test 1 with PVEE or 71.73 % for Test 4 with P-1-D.

The oil recovery factors of CO_2 thickened by using either polymer as a direct thickener at different injected pore volumes are plotted in Figure 8c. It is found that before polymer-thickened CO_2 breakthrough, the oil recovery increases drastically with the injected P.V. After injecting 0.69 P.V. for Test 3 with PVEE or 0.80 injected P.V. for Test 6 with P-1-D, the polymer-thickened CO_2 breakthrough occurs. The respective oil recovery factors are found to be 62.00 % for Test 3 with PVEE and 64.71 % for Test 6 with P-1-D, both of which are about (16 to 18) % higher than those at pure CO_2 breakthrough. After polymer-thickened CO_2 breakthrough, the oil recovery continues to increase slowly until a total of 2.00 P.V. of polymer-thickened CO_2 is injected. There is no oil production after 2.00 injected P.V. The final oil recovery factor for Test 3 with PVEE is equal to 72.96 %, which is almost 10 % lower than 82.00 % for Test 6 with P-1-D. This is because CO_2 thickened by using P-1-D at P_{cp} = 16.2 MPa has a higher viscosity than CO_2 thickened by using PVEE at P_{cp} = 15.2 MPa as shown in Figure 6, though P-1-D has a lower solubility in pure CO_2 at P_{cp} = 16.2 MPa than

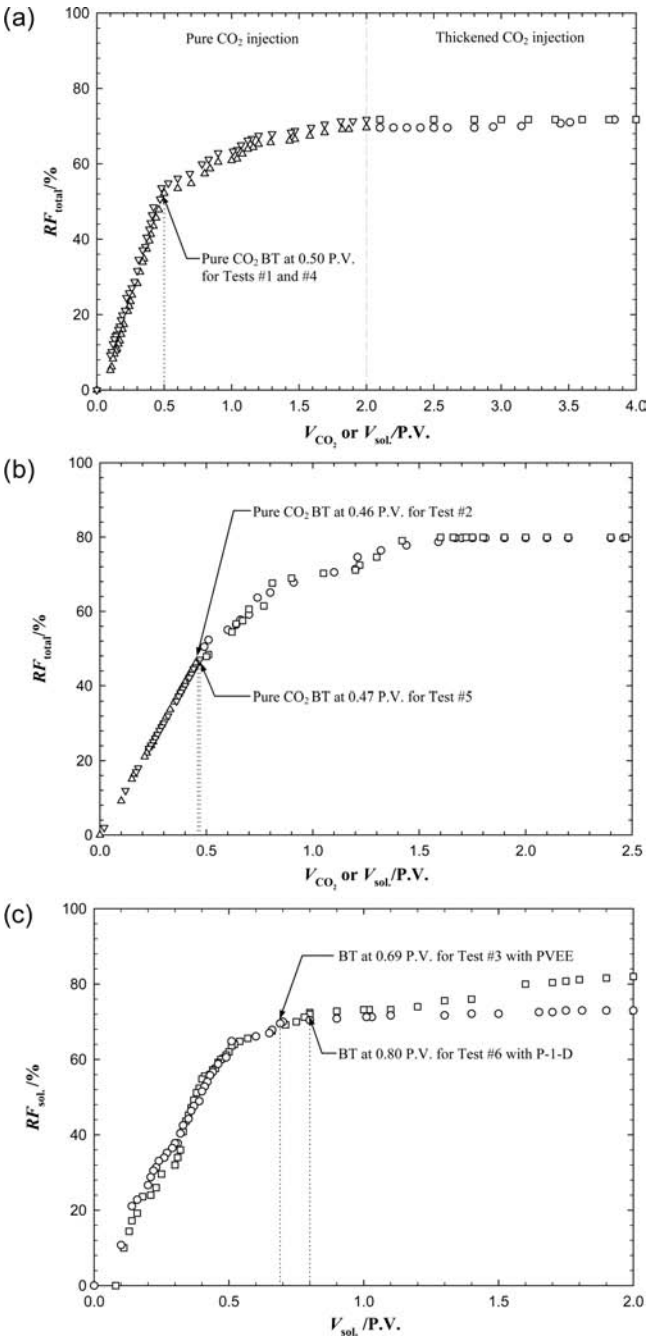

Figure 8. Measured total oil recovery factor, RF_{total}, versus injected P.V. of pure or polymer-thickened CO_2, V_{CO_2} or $V_{sol.}$, at q_{CO_2} or $q_{sol.}$ = 0.4 $cm^3 \cdot min^{-1}$ and T_{res} = 329.15 K. (a) △, pure CO_2 flooding in Test 1 at P = 15.2 MPa; ○, PVEE-thickened CO_2 flooding in Test 1 at P = 15.2 MPa; ▽, pure CO_2 flooding in Test 4 at P = 16.2 MPa; □, P-1-D-thickened CO_2 flooding in Test 4 at P = 16.2 MPa. (b) △, pure CO_2 flooding in Test 2 at P = 15.2 MPa; ○, PVEE-thickened CO_2 flooding in Test 2 at P = 15.2 MPa; ▽, pure CO_2 flooding in Test 5 at P = 16.2 MPa; □, P-1-D-thickened CO_2 flooding in Test 5 at P = 16.2 MPa. (c) Measured oil recovery factor, $RF_{sol.}$, versus injected P.V. of polymer-thickened CO_2, $V_{sol.}$, at $q_{sol.}$ = 0.4 $cm^3 \cdot min^{-1}$ and T_{res} = 329.15 K. ○, PVEE-thickened CO_2 flooding in Test 3 at P = 15.2 MPa; □, P-1-D-thickened CO_2 flooding in Test 6 at P = 16.2 MPa.

PVEE at P_{cp} = 15.2 MPa as shown in Figure 4. In comparison with Tests 1 and 4, a direct injection of polymer-thickened CO_2 achieves better oil recovery (e.g., over 1 % for Test 3 with PVEE and 10 % for Test 6 with P-1-D) than the total oil recovery of pure and polymer-thickened CO_2 flooding processes. In particular, the direct injection of P-1-D-thickened CO_2 in Test 6 results in the highest oil recovery among all of the six high-pressure CO_2 coreflood tests.

■ CONCLUSIONS

In this paper, a novel mobility-control technique is applied to enhance oil recovery in CO_2 flooding by using either PVEE or P-1-D as a direct thickener to viscosify pure CO_2. The cloud-point pressures of these two polymers in pure CO_2 are measured by using a see-through windowed high-pressure cell. The IFTs between the light crude oil and pure/polymer-thickened CO_2 are measured by applying the axisymmetric drop shape analysis technique for the pendent drop case. The polymer-thickened CO_2 viscosity is measured by using a capillary viscometer. A total of six miscible high-pressure CO_2 coreflood tests are conducted to study the effect of polymer-thickened CO_2 on the oil recovery under the actual reservoir conditions. It is found that both polymers are adequately soluble in pure CO_2. In particular, PVEE has a higher solubility in pure CO_2 than P-1-D at the same and low polymer cloud-point pressure. The measured equilibrium IFTs show that both polymers can substantially reduce the IFT at high equilibrium pressures and that the measured equilibrium IFT for the light crude oil−PVEE-thickened CO_2 system is much lower than that for the light crude oil−P-1-D-thickened CO_2 system. The measured thickened CO_2 viscosities for both polymers show their strong CO_2 viscosity enhancement abilities, especially at low polymer cloud-point pressures. P-1-D-thickened CO_2 has a high viscosity if the reservoir pressure is high enough for P-1-D to achieve an adequate solubility in pure CO_2. It is also found that the subsequent injection of PVEE-thickened CO_2 can marginally mobilize and produce the residual oil after the complete pure CO_2 flooding, whereas P-1-D-thickened CO_2 injection shows no effect. The polymer-thickened CO_2 injection can achieve a much higher oil recovery factor than pure CO_2 injection. The CO_2 breakthrough is significantly delayed when polymer-thickened CO_2 is injected from the beginning and direct injection of P-1-D-thickened CO_2 achieves the highest oil recovery factor.

■ AUTHOR INFORMATION

Corresponding Author

*Tel.: 1-306-585-4630. Fax: 1-306-585-4855. E-mail: peter.gu@uregina.ca.

Funding Sources

The authors want to acknowledge the discovery grant from the Natural Sciences and Engineering Research Council (NSERC) of Canada to Y.G.

■ ACKNOWLEDGMENT

The authors also wish to thank Ms. Xiaoqi Wang at the University of Regina for her technical assistance in conducting the high-pressure CO_2 coreflood tests and Dr. Chuanzhong Wang at the University of Regina for his technical assistance in measuring the molecular weight of P-1-D.

REFERENCES

(1) Moritis, G. Special Report: EOR/Heavy Oil Survey. *Oil Gas J.* **2006**, *104*, 37–57.

(2) Farouq Ali, S. M.; Thomas, S. The Promise and Problems of Enhanced Oil Recovery Methods. *J. Can. Pet. Technol.* **1996**, *35*, 57–63.

(3) Pyo, K.; Damian-Diaz, N.; Powell, M.; van Nieuwkerk, J. CO_2 Flooding in Joffre Viking Pool. Paper 2003-109, *Proceeding of the 4th Canadian International Petroleum Conference*, Calgary, Alberta, 2003.

(4) Aycaguer, A. C.; Lev-On, M.; Winer, A. M. Reducing Carbon Dioxide Emissions with Enhanced Oil Recovery Projects: A Life Cycle Assessment Approach. *Energy Fuels* **2001**, *15*, 303–308.

(5) Huang, E. T. S.; Holm, L. W. Effect of WAG Injection and Rock Wettability on Oil Recovery during CO_2 Flooding. *SPE Res. Eng.* **1988**, *3*, 119–129.

(6) Maini, B. B. Laboratory Evaluation of Foaming Agents for High-Temperature Applications -III. Effect of Residual Oil on Mobility Reduction Performance. Paper 86-37-01, *Proceeding of the 37th Annual Technical Meeting of the Petroleum Society of CIM*, Calgary, Alberta, 1986.

(7) Wu, X.; Ogbe, D. O.; Zhu, T.; Khataniar, S. Critical Design Factors and Evaluation of Recovery Performance of Miscible Displacement and WAG Process. Paper 2004-192, *Proceeding of the 5th Canadian International Petroleum Conference*, Calgary, Alberta, 2004.

(8) Farajzadeh, R.; Andrianov, A.; Zitha, P. L. J. Foam-Assisted Enhanced Oil Recovery at Miscible and Immiscible Conditions. Paper SPE 126410, *Proceeding of the Kuwait International Petroleum Conference and Exhibition*, Kuwait City, Kuwait, 2009.

(9) Bae, J. H. Viscosified CO_2 Process: Chemical Transport and Other Issues. Paper SPE 28950, *Proceeding of the SPE International Symposium on Oilfield Chemistry*, San Antonio, TX, 1995.

(10) Heller, J. P.; Dange, D. K.; Card, R. J.; Donaruma, L. G. Direct Thickeners for Mobility Control of CO_2 Floods. *SPE J.* **1985**, *25*, 679–686.

(11) Dandge, D. K.; Heller, J. P. Polymers for Mobility Control in CO_2 Floods. Paper SPE 16271, *Proceeding of the SPE International Symposium on Oilfield Chemistry*, San Antonio, TX, 1987.

(12) Bae, J. H.; Irani, C. A. A Laboratory Investigation of Viscosified CO_2 Process. *SPE Adv. Technol. Ser.* **1993**, *1*, 166–171.

(13) Rindfleisch, F.; DiNoia, T. P.; McHugh, M. A. Solubility of Polymers and Copolymers in Supercritical CO_2. *J. Phys. Chem.* **1996**, *100*, 15581–15587.

(14) Huang, Z.; Shi, C.; Xu, J.; Kilic, S.; Enick, R. M. Enhancement of the Viscosity of Carbon Dioxide Using Styrene−Fluoroacrylate Copolymers. *Macromolecules* **2000**, *33*, 5437–5442.

(15) Enick, R. M.; Beckman, E. J. Direct Thickeners for Carbon Dioxide. Paper SPE 59325, *Proceeding of the SPE/DOE Improved Oil Recovery (IOR) Symposium*, Tulsa, OK, 2000.

(16) Xu, J.; Wlaschin, A.; Enick, R. M. Thickening Carbon Dioxide with the Fluoroacrylate−Styrene Copolymer. *SPE J.* **2003**, *8*, 85–91.

(17) Fink, R.; Hancu, D.; Valentine, R.; Beckman, E. J. Toward the Development of "CO_2-Philic" Hydrocarbons. 1. Use of Side-Chain Functionalization to Lower the Miscibility Pressure of Polydimethylsiloxanes in CO_2. *J. Phys. Chem. B* **1999**, *103*, 6441–6444.

(18) Sarbu, T.; Styranec, T.; Beckman, E. J. Non-Fluorous Polymers with Very High Solubility in Supercritical CO_2 Down to Low Pressures. *Nature* **2000**, *405*, 165–168.

(19) Kilic, S.; Michalik, S.; Wang, Y.; Johnson, J. K.; Enick, R. M.; Beckman, E. J. Phase Behavior of Oxygen-Containing Polymers in CO_2. *Macromolecules* **2007**, *40*, 1332–1341.

(20) Shen, Z.; McHugh, M. A.; Xu, J.; Belardi, J.; Kilic, S.; Mesiano, A.; Bane, S. E.; Karnikas, C.; Beckman, E. J.; Enick, R. M. CO_2 Solubility of Oligomers and Polymers that Contain the Carbonyl Group. *Polymer* **2003**, *44*, 1491–1498.

(21) Trapriyal, D.; Wang, Y.; Johnson, J. K.; Thies, M. C.; Paik, I. H.; Hamilton, A. D.; Enick, R. M. Poly(vinyl acetate), Poly((1-*O*-(vinyloxy) ethyl-2,3,4,6-tetra-*O*-acetyl-β-D-glucopyranoside) and Amorphous Poly(lactic acid) are the Most CO_2-Soluble Oxygenated Hydrocarbon-Based Polymers. *J. Supercrit. Fluids* **2008**, *46*, 252–257.

(22) Gu, Y.; Yang, D. Interfacial Tensions and Visual Interactions of Crude Oil−Brine−CO_2 Systems Under Reservoir Conditions. Paper 2004-083, *Proceeding of the 5th Canadian International Petroleum Conference*, Calgary, Alberta, 2004.

(23) Cheng, P.; Li, D.; Boruvka, L.; Rotenberg, Y.; Neumann, A. W. Automation of Axisymmetric Drop Shape Analysis for Measurements of Interfacial Tension and Contact Angles. *Colloids Surf.* **1990**, *43*, 151–167.

(24) Peng, D. Y.; Robinson, D. B. A New Two-Constant Equation of State. *Ind. Eng. Chem. Fundam.* **1976**, *15* (1), 58–64.

(25) ASTM D86, *Standard Test Method for Disstillation of Petroleum Products at Atmospheric Pressure*; ASTM International: West Conshohocken, PA, 2003.

(26) Meilchen, M. A.; Hasch, B. M.; McHugh, M. A. Effect of Copolymer Composition on the Phase Behavior of Mixtures of Poly(ethylene-co-methyl acrylate) with Propane and Chlorodifluoromethane. *Macromolecules* **1991**, *24*, 4874–4882.

(27) Harrison, K. L.; Johnston, K. P.; Sanchez, J. S. Effect of Surfactants on the Interfacial Tension between Supercritical Carbon Dioxide and Polyethylene Glycol. *Langmuir* **1996**, *12*, 2637–2644.